

Electronically stimulated adsorbate dissociation in the presence of an electronegative coadsorbate: (NO₂ + O) on Pt(111)

T. M. Orlando,* A. R. Burns, D. R. Jennison, and E. B. Stechel
Sandia National Laboratories, Division 1151, Albuquerque, New Mexico 87185
 (Received 3 September 1991; revised manuscript received 2 December 1991)

The effects of an electronegative coadsorbate on the stimulated dissociation of a chemisorbed molecule are investigated using state-resolved laser-ionization spectroscopy of those dissociation fragments which leave the surface. Specifically, we examine the NO(²Π_{Ω=1/2,3/2}) and O(³P_J) fragment energies and yields resulting from electron- (6–350 eV) stimulated dissociation of chemisorbed NO₂ as a function of preadsorbed atomic O coverage. The most dramatic effect associated with O coverage (up to Θ_O=0.75 monolayer) is a large (a factor of 26) enhancement in the specific NO₂ dissociation yield. There is also an O-induced narrowing of the translational energy distributions and a decrease in both the rotational and vibrational energy of the NO fragment. The dissociation threshold of ~10 eV, together with lifetime arguments, suggest that the dominant excitation(s) are shallow-valence two-hole excitations. The above observations can be understood in terms of reduced substrate charge-transfer screening of these excitations. In addition, we observe a distinct propensity (>4:1 at low *J*) for populating the upper (Ω=3/2) over the lower (Ω=1/2) level of the spin-orbit-split NO(²Π_Ω) ground state, whereas the spin-orbit population of the O(³P_J) fragment is statistical (2*J*+1) within experimental error. The O(³P_J) yield derives from dissociation of nitro-bound NO₂ (N end down); no O(³P_J) yield can be associated with side-bonded NO₂.

I. INTRODUCTION

Irradiation of surfaces with energetic electrons and photons produces electronic excitations which may stimulate the desorption or dissociation of molecular adsorbates. The basic physics involved in stimulated desorption,^{1–4} dissociation,^{5–14} and reactions^{15–18} has been probed in several recent investigations. Stimulated dissociation has been shown to occur from at least three different mechanisms, which may act separately or collectively.^{10,19} The first mechanism involves direct excitation of the bulk substrate followed by “hot” carrier-induced dissociation.^{7,8} In the second mechanism, which is applicable to weakly bound adsorbates or multilayers, a direct dissociative excitation of the adsorbate occurs.^{10,14} A third mechanism, which applies to more strongly chemisorbed adsorbates, involves the creation of electronic excitations in the rehybridized adsorbate-substrate complex.^{5,6,12} In all of the above, the dissociative yield is strongly dependent upon the nature of the adsorbate-substrate coupling in both the ground and excited states.^{8,20,21} In the present study, the yield and dynamics of the third mechanism will be examined in the presence of an electronegative coadsorbate which directly modifies the electronic environment at the adsorbate complex.

For molecules chemisorbed on transition metals, the lifetimes of excitations may be intimately coupled to substrate screening which involves charge transfer to the adsorbate. This is especially true when intra-atomic Auger processes use a screening charge in the decay of the excitation.^{1,5,6,23} Decay via resonant tunneling from the substrate, while typically much faster than Auger rates, is forbidden for excitations whose energy falls below the

valence band of the substrate.^{1,5,6,15,23} In addition to lifetime effects, which strongly influence yields, charge-transfer screening also alters the degree of internal (vibrational and rotational) excitation of the departing neutral products, particularly if the screening charge occupies antibonding molecular orbitals of the excited adsorbate.^{1,5,6,23}

Since coadsorbates can modify substrate charge-transfer screening it is of great interest to probe not only coadsorbate effects on yields of stimulated surface processes but also on the internal states of the products.^{22,23} A recent study of the electron-stimulated desorption (ESD) of chemisorbed NO from Pt(111) demonstrated that the ESD yield increases by more than a factor of 90 in the presence of coadsorbed atomic O.²³ The effects of coadsorbed atomic oxygen on the NO ESD from Pt(111) were explained²³ primarily in terms of an increased lifetime of a single excitation (5σ⁻¹ hole) which was brought about by an O-induced reduction in charge-transfer screening into the antibonding 2π molecular orbital of NO. Since this screening charge is used in the dominant Auger decay channel, a reduction in the charge-transfer screening resulted in both a reduced decay rate (hence an enhanced lifetime) and a reduction in the vibrational energy of the NO desorbate.

The adsorption of NO₂ on clean (no preadsorbed O atoms) and O-covered Pt(111) has been characterized by Bartram, Windham, and Koel^{24,25} using vibrational spectroscopy and temperature-programmed desorption. At temperatures below 150 K, NO₂ adsorbs molecularly on the clean surface in a μ-N,O-nitrito complex.²⁵ In this configuration, which we henceforth call the “side-bonded” geometry, NO₂ is coordinated to Pt bridge sites

through the nitrogen and one oxygen; the other oxygen points away from the surface. At high coverages of preadsorbed atomic oxygen (Θ_{O}), the NO_2 coordination is thought to be "nitro," i.e., through the nitrogen at Pt atop sites with both oxygen atoms pointing away from the surface.²⁴ We henceforth call this the "N-bonded" geometry. Both side-bonded and N-bonded geometries are present at intermediate O coverages. There is no evidence of NO_3 or N_2O_4 formation at any Θ_{O} at temperatures > 155 K (Ref. 24) and no evidence of O_2 formation for Θ_{O} up to the maximum of $\Theta_{\text{O}}=0.75$ monolayer (ML) (Refs. 24, 26, and 27), where $\Theta_{\text{O}}=1$ is equal to the atomic density of the Pt(111) surface. Given these geometrical changes and the $+0.5$ -eV increase in the Pt(111) work function for $\Theta_{\text{O}}=0.75$ ML, relative to the clean surface,²⁷ it is clear that the oxygen modifies the local electronic environment.

The electron-stimulated dissociation of side-bonded NO_2 on clean Pt(111) has been studied previously^{5,6} using state-specific detection of the NO dissociation product. Evidence for two excitation channels with comparable thresholds (~ 10 – 11 eV) and yields was presented.⁵ It was suggested that one channel involves the excitation of a $3b_2$ electron, while the other channel involves a two-electron excitation from the $1a_2$ level.⁵ Evidence for both of these channels was seen in the changes in the NO-fragment translational-energy distributions with both vibrational and rotational energy, which might result from differences in the substrate screening charge and the subsequent excited-state forces for the two channels.

Analogous to the ESD of NO discussed above, here we find that the presence of coadsorbed O not only results in an enhanced dissociation yield relative to the clean surface, but also causes significant changes in the NO fragment translational, vibrational, and rotational energy distributions. We also observe a definite propensity for populating the $\Omega=\frac{3}{2}$ spin-orbit state (120 cm^{-1} above the $\Omega=\frac{1}{2}$ level), of the open-shell $^2\Pi_{3/2,1/2}$ ground-state NO molecule. We show that most of our observations can be explained in terms of the adsorbate geometry change and reduced substrate charge-transfer screening of the primary excitation(s). We suggest that the O-induced reduction of screening leads to a significant increase in the lifetime of the two-hole excitation observed for NO_2 dissociation on clean Pt(111). Finally, we consider the spin-orbit propensity in light of the Pt(111) electronic structure and NO_2 adsorption geometry.

II. EXPERIMENT

The experimental arrangement for laser resonance-enhanced multiphoton ionization (REMPI) detection of neutral products from ESD and stimulated dissociation has been published elsewhere.^{1,5,6} Briefly, all the experiments discussed below have been performed with an ion-pumped vacuum chamber having a base pressure below 5×10^{-11} Torr. The chamber is equipped with a cylindrical mirror analyzer for Auger electron spectroscopy (AES), a quadrupole mass spectrometer for thermal-desorption spectrometry (TDS), a pulsed electron gun,

and a time-of-flight (TOF) apparatus for the detection of ions produced via REMPI. All experiments are done in the TOF mode whereby the neutral particles produced by a 0.3 – 1.0 - μs (variable) electron-beam pulse (1.6×10^{16} electrons/ cm^2s) traverse a 0.5 -cm distance before they are resonantly ionized at a variable time delay by the 4 -ns laser pulse.

The polished Pt(111) crystal can be resistively heated to 1200 K and cooled to 90 K. The crystal is initially cleaned by Ar^+ -ion bombardment and annealed at 1200 K; cleanliness of the crystal is confirmed at the 1% level by the absence of $C(KLL)$ and $O(KLL)$ transitions in the AES. The clean Pt(111) surface is precovered with O using a technique initially described by Segner, Vielhaber, and Ertl²⁶ which involves exposure of the crystal to NO_2 at 400 K. At this temperature, NO_2 thermally dissociates producing O-atom coverages up to $\Theta_{\text{O}}=0.75$ ML, as verified by the 0.90 ratio of the AES peak heights $I(O(KLL))/I(\text{Pt}(238\text{ eV}))$ at the highest Θ_{O} .^{24,26,27} Previous workers^{26,27} have shown that at $\Theta_{\text{O}}=0.25$ ML, the atomic O occupies threefold hollow sites giving rise to a $p(2 \times 2)$ ordered array which is lost as Θ_{O} increases. At $\Theta_{\text{O}}=0.75$ ML, the $p(2 \times 2)$ is visible but faint, indicating the onset of one-dimensional disorder.²⁷ All oxygen coverages produced by this method are determined by AES before subsequently chemisorbing molecular NO_2 for the coadsorption experiments; the depletion of the O layer due to the Auger electron beam is negligible.

The NO_2 gas is handled in a passivated stainless-steel manifold which is equipped with a glass cold finger for freeze-pump-thaw degassing. The chamber pressure never exceeds $\sim 2 \times 10^{-10}$ Torr during dosing through a passivated effusive source in front of the sample. Molecular adsorption of NO_2 on clean Pt(111) is confirmed by examining the TDS, which qualitatively reproduces previous data.²⁴ Direct detection of the desorbed NO_2 (mass 46) is difficult due to the non-line-of-sight location of the quadrupole mass spectrometer and extensive cracking in the ionizer. Except for the large multilayer ice peak (~ 150 K) which can readily be seen at mass 46, we find that the NO_2 TDS features are observed more easily as NO (mass 30). During NO_2 dosing, the crystal temperature is kept at 165 K in order to prevent both the formation of an ice layer and thermal dissociation. Saturation- NO_2 coverage on the clean surface is 0.5 ML.²⁵ Uptake curves²⁴ indicate that at intermediate Θ_{O} , saturated NO_2 coverage is roughly inversely proportional to Θ_{O} such that at $\Theta_{\text{O}}=0.75$ ML, the NO_2 coverage is approximately 0.15 ML. The crystal is cooled to 90 K before data acquisition.

State-specific TOF translational energy (E_{trans}) distributions are obtained by computer-programmed steps in the delay time between the electron-beam pulse ($0.3\ \mu\text{s}$) and the laser pulse.^{1,5,6} The data are automatically scaled in energy and have been corrected for the velocity dependence of the neutral particle density in the laser focal volume; however, there exists an intrinsic error due to the velocity spread (Δ_v/v) which arises from the electron-beam pulse width. Thus the TOF E_{trans} distributions are best suited for observing relative changes (e.g.,

O-induced).

Threshold energy measurements are obtained by sweeping the electron-beam energy (E_{HV} , where HV is the accelerating high voltage) at a fixed E_{trans} (i.e., fixed delay time). Both the energy sweep and electron-beam focusing are computer controlled to ensure a constant spot size (0.016 cm^2) and current density incident on the sample (0.78 cm^2) for $E_{\text{HV}} > 20 \text{ eV}$. At $E_{\text{HV}} < 20 \text{ eV}$, the beam current remains constant, but the spot size increases. To ensure that the threshold data refers *only* to molecules which are on the crystal surface, the background signal which may arise from molecules on the crystal mounts is subtracted out. The background signal is obtained by repeating the scan after thermally desorbing all of the NO_2 from the Pt(111) substrate at 400 K.

The NO fragment is detected by scanning through the $A^2\Sigma^+(\nu') \leftarrow X^2\Pi_{1/2,3/2}(\nu)$ resonance-enhanced (1+1) ionization.^{28,29} For NO ($\nu=0, 1, 2,$ and 3) the laser is focused with a cylindrical lens into a ribbon-shaped beam area of $\sim 0.5 \text{ cm}^2$ which angle-integrates most of the neutral particles leaving the surface. Possible saturation and alignment effects²⁹ are calibrated by comparison of calculated rotational line-strength intensities³⁰ with the measured room-temperature $A^2\Sigma^+(\nu'=0) \leftarrow X^2\Pi_{1/2,3/2}(\nu''=0)$ transition intensities which are obtained by backfilling the chamber with NO.

The two-photon resonant $3p^3P_{2,1,0} \leftarrow 2p^3P_{2,1,0}$ transitions ($225.7\text{--}226.2 \text{ nm}$), followed by single-photon ionization, in an overall (2+1) laser ionization scheme³¹ are used to detect $\text{O}(^3P_J)$ fragments. The laser beam (0.5 mJ) is focused tightly by a 6.0-in. spherical lens to a spot 0.5 cm above the surface. The power density in this focal volume ensured that the $\text{O}(^3P_J)$ transitions are completely saturated. Based on the NO results, we estimate our $\text{O}(^3P_J)$ detection sensitivity of $\sim 10^6 \text{ atoms/cm}^3$ quantum state, which places our *detection* limit for neutral $\text{O}(^3P_J)$, produced by stimulated desorption or dissociation, to events which have cross sections $\sim 10^{-19} \text{ cm}^2$. Data are collected with laser pulse energies that were within $\pm 15\%$ of a mean laser energy as determined by a pyroelectric detector.

III. RESULTS

All data presented here, except for the thresholds, are *independent* of electron-beam energies ranging from ~ 25 to 350 eV . Due to higher excitation cross section and contributions from secondary electrons, most of the TOF data presented are obtained using an electron-beam energy of 350 eV . Rotational spectra are obtained at 50 eV to eliminate significant erosion during longer data-acquisition periods.

A. NO_2 dissociation yield vs Θ_{O}

As seen in Fig. 1, the specific NO_2 dissociation yield (350-eV electron-beam energy) is shown to increase dramatically as a function of preadsorbed atomic oxygen. Specific NO ($\nu=0$) yields are obtained by integrating over the translational energy distributions (some of which are displayed in Fig. 3) and normalizing the sum by the

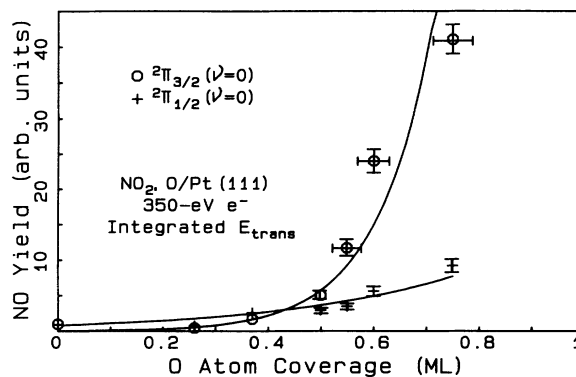


FIG. 1. Enhancement in the specific NO_2 dissociation yield as a function of O-atom coverage on Pt(111). The specific dissociation yield for each spin-orbit level of the NO ground state is obtained by dividing the integrated TOF E_{trans} distributions taken at the $^2\Pi_{3/2}(\nu=0)P_{12}$ and $^2\Pi_{1/2}(\nu=0)P_{11}$ bandheads by the NO_2 coverage. The solid curves are single exponential fits.

NO_2 coverage. After adding together the intensities for the two spin-orbit levels at each Θ_{O} , the overall specific yield is found to increase by a factor of 26 from the clean surface to saturation $\Theta_{\text{O}}=0.75 \text{ ML}$. Although this is a significantly large increase, this overall enhancement is substantially less than that (90-fold) observed for ESD of NO from Pt(111) at the same oxygen coverages.^{6,23} In Ref. 5, the cross section for the 350-eV electron-stimulated dissociation of NO_2 on clean Pt(111) was estimated to be $\sim 5 \times 10^{-18} \text{ cm}^2$. The factor-of-26 enhancement in the specific dissociation yield implies an overall cross section with $\Theta_{\text{O}}=0.75 \text{ ML}$ of $\sim 10^{-16} \text{ cm}^2$. This value is several orders of magnitude higher than the typical cross-section values for surface photochemistry ($\sim 5.7 \times 10^{-20} \text{ cm}^2$ at 5.4-eV photon energy¹¹) and for photoinduced dissociative electron attachment reactions [$\sim 10^{-20}\text{--}10^{-19} \text{ cm}^2$ (Ref. 7)]. However, it should be noted that for the present results, the cross sections may have significant contributions from secondary electrons.

On clean Pt(111), evidence was presented⁵ which demonstrated that most of the O-atom fragments of NO_2 dissociation remained on the surface. Given the coordination of the O atom in the NO_2 side-bonded geometry,²⁵ this behavior is consistent with preferential breaking of the N-O bond which is parallel to the surface and which would be expected to have a lower barrier to dissociation. However, with increasing Θ_{O} , N-bonded NO_2 prevails²⁴ and it is reasonable to expect that O-atom dissociation fragments from this species would leave the surface. This can be seen in Fig. 2, where the ground-state $\text{O}(^3P_J)$ gas-phase yield increases dramatically on the O-covered surface relative to the clean surface. All three J levels were detected (Sec. III D 2), but the $J=2$ line is the most intense. We attribute the O yield to the N-bonded NO_2 dissociation. Absolutely no ESD of preadsorbed O was detected with $25\text{--}350\text{-eV}$ electron bombardment of Pt(111) within our detection sensitivity of 10^{-19} cm^2 . Furthermore, ESD of preadsorbed O is *not* induced by the presence of coadsorbates since no $\text{O}(^3P_2)$ is detected with 350-eV electron-irradiation of either NO coadsorbed

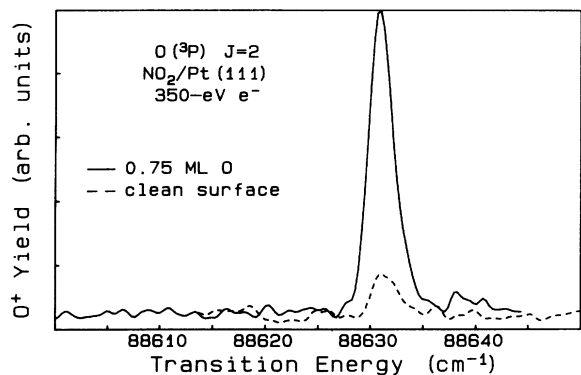


FIG. 2. Comparison of the $O(^3P_2)$ yields produced in the electron-stimulated dissociation of NO_2 on Pt(111) containing $\Theta_{\text{O}}=0.75$ ML (solid curve) and on clean Pt(111) (dotted curve). The NO_2 coverage is 0.15 ML on the O-covered surface and 0.55 ML on the clean surface.

with $\Theta_{\text{O}}=0.75$ ML or O_2 coadsorbed with $\Theta_{\text{O}}=0.50$ ML on Pt(111).³²

Any yield of $O(^3P_2)$ from the clean surface is surprising considering the side-bonded geometry. The small $O(^3P_2)$ yield may be due to traces of N-bonded NO_2 which may be created by excessive (greater than saturation) exposure of the clean surface to NO_2 . This idea is supported by our observation of an appreciable reduction of this $O(^3P_2)$ yield after heating the surface containing only NO_2 to 175 K for several minutes. Since side-bonded NO_2 is still present at large quantities at 175 K, this cannot be the adsorbate species producing the detected O atoms. Trace N-bonded NO_2 may also explain the small NO_2 160-K desorption peak which is detectable after NO_2 exposures greater than 2.9 langmuirs at 100 K.²⁵ Given the temperature-dependent yield of the O atom on the clean surface, it is not possible at this time to correlate it with the increased dissociation yield, which we believe is due to lifetime effects (Sec. IV B).

It should be pointed out that long-lived excited-state O fragments such as $O(^1D)$ and $O(^1S)$ may also be formed.^{33,34} Both of these species are, in principle, amenable to REMPI detection: $O(^1D)$ is 2 eV above the ground-state $O(^3P_J)$ and has a lifetime of 150 sec, whereas $O(^1S)$ is 4.2 eV above the ground state and has a lifetime of 0.8 s. However, unknown two-photon cross sections and ionization rates, coupled with competitive autoionization processes,³⁴ prohibit a quantitative assessment of the relative excited-state populations.

B. NO, O fragment translational energies

TOF E_{trans} distributions of $\text{NO } ^2\Pi_{\Omega=3/2}(\nu=0)$ dissociation fragments for several preadsorbed atomic oxygen coverages are presented in Fig. 3. These distributions, which are normalized at their maxima, have pronounced variations in their widths depending on Θ_{O} . The broad distribution characteristic of the $\text{NO } ^2\Pi_{3/2}(\nu=0)$ fragment produced from the dissociation of NO_2 on clean Pt(111) collapses to a narrow distribution at $\Theta_{\text{O}}=0.75$ ML. The low- E_{trans} energies disappear “first,” i.e., at a

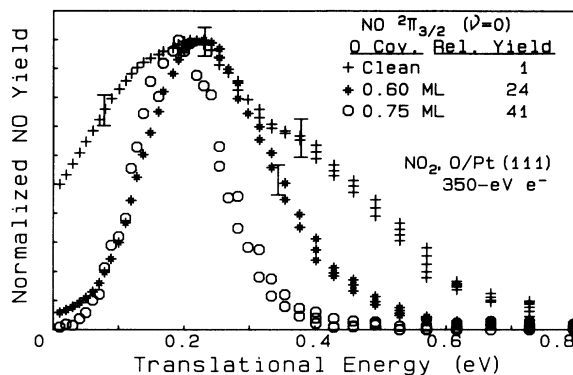


FIG. 3. Normalized TOF E_{trans} distributions for the $\text{NO } ^2\Pi_{3/2}$ fragment of electron-stimulated dissociation of NO_2 on Pt(111) as a function of O-atom coverage (Θ_{O}). The data were acquired at the $\text{NO } \nu=0, J=9.5-11.5 P_{12}$ bandhead.

lower Θ_{O} than do the high- E_{trans} energies. Comparison of the normalized E_{trans} distributions for $\text{NO } ^2\Pi_{1/2}$ and $^2\Pi_{3/2}$ at $\Theta_{\text{O}}=0.75$ ML is shown in Fig. 4. The peak and high energies are the same, and a similar collapse of the width of both spin-orbit states occur as a function of Θ_{O} . In the normalized data of Fig. 4, there is apparently a higher relative yield for the $\text{NO } ^2\Pi_{1/2}$ fragment at low E_{trans} . In actuality (see inset of Fig. 4), the $\Omega=\frac{3}{2}, \frac{1}{2}$ yields at low E_{trans} are similar on an absolute scale, reflecting the fact that the spin-orbit propensity is lost at the lowest E_{trans} . In the ESD of NO from clean and O-covered Pt(111), the E_{trans} distributions of the $\Omega=\frac{1}{2}$ and $\frac{3}{2}$ levels behave similarly, whereas in the laser desorption of NO from clean Pt(111),³ the $\Omega=\frac{3}{2}$ distributions are peaked at significantly higher energies than those for the $\Omega=\frac{1}{2}$ spin-orbit level.

As mentioned in Sec. I, vibrationally and rotationally excited NO fragments⁵ from NO_2 dissociation on clean Pt(111) are observed at higher E_{trans} energies. Associated with this is a “bimodal” NO E_{trans} distribution at moderate ($J \equiv 16.5$) rotational energies.⁵ These observa-

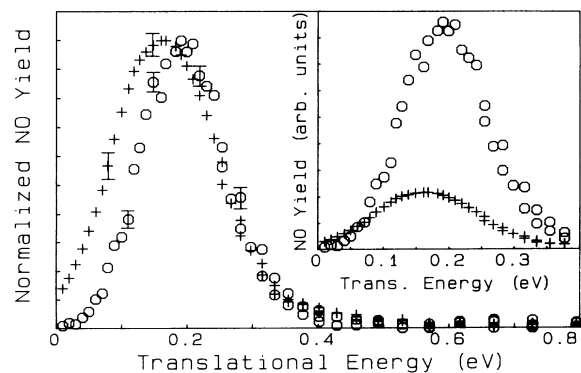


FIG. 4. Comparison of the *normalized* TOF E_{trans} distributions for the $\text{NO } ^2\Pi_{1/2}$ (+) and $^2\Pi_{3/2}$ (o) fragments of NO_2 electron-stimulated dissociation on O-covered ($\Theta_{\text{O}}=0.75$ ML) Pt(111). Inset: Same data plotted on an *absolute* (unnormalized) scale. Data were taken at the $\nu=0, J=8.5-10.5 P_{11}$ and $\nu=0, J=9.5-11.5 P_{12}$ bandheads.

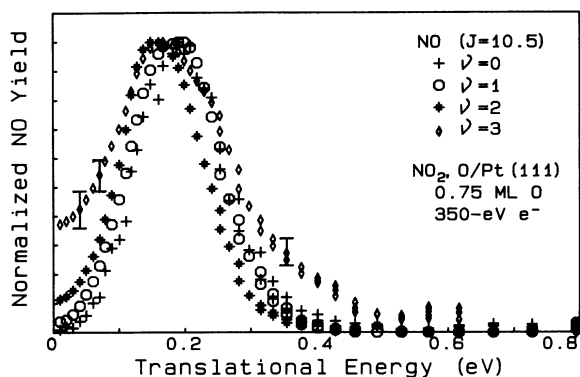


FIG. 5. Normalized TOF E_{trans} distributions for vibrationally resolved ($\nu=0, 1, 2, 3$) ${}^2\Pi_{3/2}$ NO dissociation fragments of NO_2 dissociation on O-covered ($\Theta_{\text{O}}=0.75$ ML) Pt(111). The data were acquired at the P_{12} bandheads ($J=9.5\text{--}11.5$).

tions, and the broad TOF E_{trans} seen in Fig. 3, for $\nu=0$, $J\sim 9.5$, suggest that at least two distinct channels are involved in the dissociation event on clean Pt(111).⁵ However, for $\Theta_{\text{O}}=0.75$ ML, the narrower ${}^2\Pi_{3/2}$ E_{trans} distributions for $\nu=0, 1, 2$, and 3 shown in Fig. 5 all peak at the same energy and have similar widths. The only exception is the width of the $\nu=3$ distribution, which is probably due to the very low signal of this small population. Similarly, the NO ${}^2\Pi_{3/2}$ ($\nu=0$) E_{trans} distributions vs rotational energy (see Fig. 6) are unchanged from $J=1.5$ to 16.5, while there is a slight shift to higher E_{trans} for $J > 20.5$. This behavior for both vibrationally and rotationally resolved E_{trans} distributions is also observed for the ESD of NO from a $\Theta_{\text{O}}=0.75$ -ML-covered Pt(111) surface, where it is believed that one desorption channel is dominant.²³ Since the E_{trans} distributions are relatively independent of internal energy (except at high J) and collapse to a rather narrow width, these results suggest a single dissociative channel on the O-covered surface.

The E_{trans} distribution of the $\text{O}({}^3P_2)$ fragment is shown

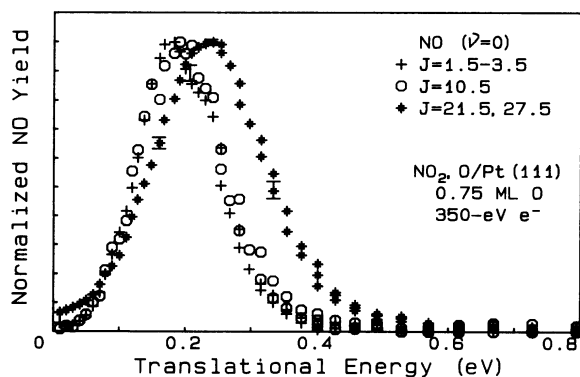


FIG. 6. Normalized TOF E_{trans} distributions for rotationally resolved ${}^2\Pi_{3/2}$ NO dissociation fragments of NO_2 dissociation on O-covered ($\Theta_{\text{O}}=0.75$ ML) Pt(111). The low- J (1.5–3.5) data were acquired at the $P_{22}Q_{12}$ bandhead, the intermediate- J data were acquired at the P_{12} bandhead ($J=9.5\text{--}11.5$), and the high- J data were acquired at the R_{22} ($J=21.5$) line that is unresolved from the $R_{12}Q_{22}$ ($J=27.5$) line.

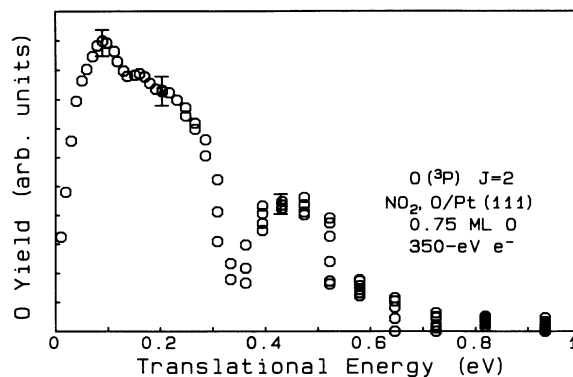


FIG. 7. Normalized TOF E_{trans} distribution of the $\text{O}({}^3P_2)$ fragment produced from electron-stimulated dissociation of NO_2 coadsorbed with $\Theta_{\text{O}}=0.75$ ML on Pt(111).

in Fig. 7. Due to signal-to-noise problems inherent in the inefficient (2+1) ionization process, the $\text{O}({}^3P_2)$ TOF E_{trans} distribution is measured only with a laser beam tightly focused with a spherical lens which does not angle-integrate the O atom flux. Thus direct comparison with the angle-integrated NO E_{trans} distributions (using a cylindrical lens) should not be done.

C. NO_2 dissociation threshold at $\Theta_{\text{O}}=0.75$ ML

In the threshold measurements, it is assumed that the final state of the primary electron is at the Fermi level. In this case, the excitation energy is given by the sum of primary-beam energy (E_{HV}) and the work function of cathode. As seen in Fig. 8, the threshold energy for the NO_2 dissociation is somewhat ambiguous in the $\nu=0$ signal of the NO fragment; however it becomes clearly defined at 9–10 eV for the $\nu=1$ and 2 levels. A similar threshold in the 10-eV range for the production of NO $\nu=0, 1$, and 2 from NO_2 dissociation on clean Pt(111) has been observed. Since possible shallow-valence excitations associated with the ill-defined $\nu=0$ threshold are not ob-

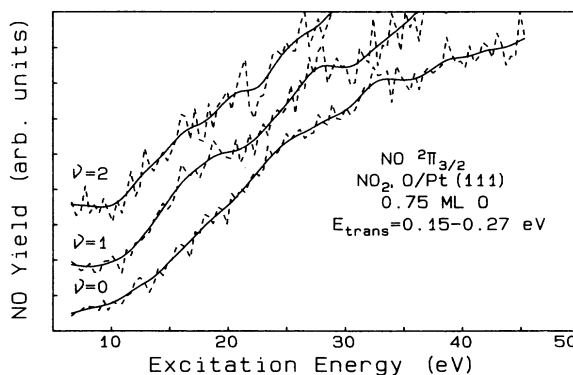


FIG. 8. Normalized thresholds (solid line is smoothed, dotted line is unsmoothed) for the production of NO in the $\nu=0, 1$, and 2 vibrational levels from the dissociation of NO_2 on Pt(111) precovered with 0.75-ML O. The excitation energy is given by $E_{\text{HV}} + \phi_c$, where E_{HV} is the electron energy and ϕ_c is the work function of the electron gun cathode.

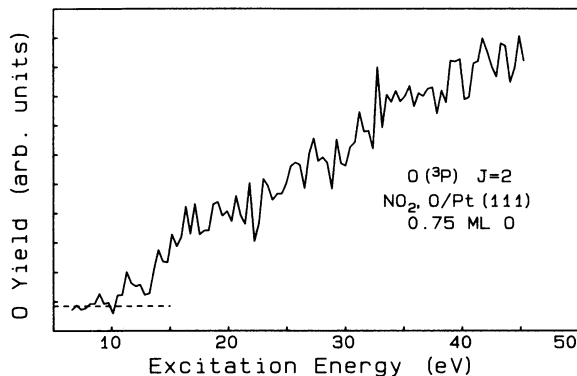


FIG. 9. The excitation energy threshold for the production of the $O(^3P_2)$ fragment of NO_2 dissociation on $\Theta_{\text{O}}=0.75$ ML precovered Pt(111). The excitation energy is given by $E_{\text{HV}} + \phi_c$, where E_{HV} is the electron energy and ϕ_c is the work function of the electron gun cathode.

served on the clean surface or in the $\nu=1$ or 2 thresholds, the *dominant* excitation(s) leading to NO_2 dissociation must be associated with the higher 9–10 eV thresholds. This is confirmed by the fact that we observe a threshold of ~ 9 –10 eV for the production of the ground-state $O(^3P_J)$ fragment. This threshold is shown in Fig. 9 and is qualitatively similar to the threshold data obtained for the production of vibrationally excited fragments, suggesting that *both* O and NO fragments are produced by the same surface dissociation event.

D. Fragment internal energies

A summary of the measured rotational- and vibrational-state distributions of the NO fragment produced from $\text{NO}_2(\dot{a})$ on clean and O-precovered Pt(111) surfaces is presented in Table I. It is relevant to point out that the fragment NO internal-state distributions are much colder than those found in NO_2 gas-phase photodissociation.³⁵ We have also measured the spin-orbit distribution of the $O(^3P_J)$ fragment at $\Theta_{\text{O}}=0.75$ ML.

TABLE I. Comparison of the NO fragment internal energies produced from electronically stimulated dissociation of NO_2 adsorbed on O-covered ($\Theta_{\text{O}}=0.75$ ML) Pt(111) and clean Pt(111). In all cases, the data were acquired at the peak E_{trans} energy (~ 0.2 eV).

	Vibrational distribution	Rotational energy (K)
	$(\text{NO}_2 + \text{O})/\text{Pt}(111)$	
$\nu=0$	1.00	560 ± 84
$\nu=1$	0.86	703 ± 105
$\nu=2$	0.16	
$\nu=3$	0.15	
	$\text{NO}_2/\text{Pt}(111)^a$	
$\nu=0$	1.00	862 ± 30
$\nu=1$	0.96	821 ± 35
$\nu=3$	0.52	743 ± 29

^aData from Ref. 5, acquired at 350-eV excitation.

1. NO spin-orbit propensity

A distinct O-coverage dependent propensity for populating the $\text{NO } ^2\Pi_{\Omega}(\nu=0)$ product in the upper spin-orbit level ($\Omega=\frac{3}{2}$) can be seen in Fig. 1. In this measurement, the laser is tuned to the P_{12} ($^2\Pi_{3/2}$) and P_{11} ($^2\Pi_{1/2}$) band heads which are mainly composed of intermediate $J=9.5$ –11.5 states. This propensity has been found to be strongly J dependent and disappears by about $J=20.5$. This is much lower than the J where the spin-orbit sublevels mix due to crossover from Hund's case (a) to case (b).^{23,28} Hence there is a dynamically significant "dilution" of the propensity at high J .

This propensity is *not* observed in either the dissociation event on a clean Pt(111) surface⁵ or in gas-phase photodissociation at the wavelengths used in this study.³⁵ However, a similar NO spin-orbit propensity is observed for ESD of NO from O-covered Pt(111) (Ref. 23) and from laser desorption of NO from clean Pt(111).³ In both desorption experiments, the $\Omega=\frac{3}{2}$ propensity is about 3:1 over $\Omega=\frac{1}{2}$ at the low- J (< 9.5) bandheads; however, for NO_2 surface dissociation at $\Theta_{\text{O}}=0.75$ ML, the propensity at low J is slightly larger ($> 4:1$). In addition, the above-mentioned dilution of the propensity is complete at $\sim J=20.5$ for stimulated dissociation rather than at $J=25.5$ as observed for NO ESD from O-precovered Pt(111).²³ These observations together imply that the spin-orbit propensity is a direct result of dissociation *on the surface*.

2. $O(^3P_{J=2,1,0})$ spin-orbit distribution

Digital integration of the $O(^3P_J)$ fine-structure spectra (A) presented in Fig. 10 yields a spin-orbit state distribution (5.0):(2.5):(1.0) for $J=2, 1,$ and 0, respectively, at $\Theta_{\text{O}}=0.75$ ML. The estimated error limits are as follows: $\pm 10\%$, $\pm 12\%$, and $\pm 15\%$ for $J=2, 1,$ and 0, respectively. Thus, this distribution is within experimental error of the $2J+1$ statistical limit of (5.0):(3.0):(1.0). For comparison under identical experimental conditions, we have also examined the $O(^3P_J)$ spin-orbit-state distribution produced from photodissociation of gas-phase NO_2 . In

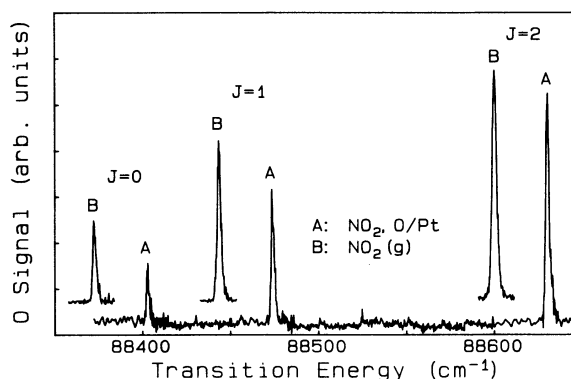


FIG. 10. Spectra of the $O(^3P_J)$ spin-orbit-state distribution produced during (a) the 350-eV electron-stimulated dissociation of NO_2 coadsorbed with $\Theta_{\text{O}}=0.75$ ML on Pt(111), and (b) 226-nm photodissociation of gas-phase NO_2 .

this experiment, the same laser pulse was used for dissociation and REMPI detection of the $O(^3P_J)$ spin-orbit-state distribution which is presented in spectrum *B* of Fig. 10. It is interesting to note that the distribution, (5.0):(2.8):(1.3) for $J=2, 1,$ and $0,$ respectively, is different from the surface dissociation in the reproducible overpopulation of $J=0.$ This is consistent with two recent gas-phase experiments which probed $O(^3P_J)$ -state distributions from 226-nm NO_2 photolysis using laser-induced fluorescence.^{36,37}

3. NO rotational energy

Analysis of the NO rotational spectra are complicated by the $^2\Pi_{3/2}$ propensity and its dilution with $J.$ Thus the most straightforward approach to determine the average rotational energy is to *sum* the $\Omega=\frac{3}{2}$ and $\Omega=\frac{1}{2}$ intensities. (Since the flux of the departing dissociation fragments is only $\sim 1 \times 10^{14}$ molecules/cm²s, molecular collisions above the substrate are negligible.) From the slope of $\ln[I(J)/(2J+1)]$ vs total rotational energy (E_{rot}), we obtain an average rotational energy of 560 ± 84 K for $\nu=0$ and 703 ± 105 K for $\nu=1.$ Spectra for $\nu=2$ and 3 are too weak for an accurate rotational analysis. As indicated in Table I, the mean rotational energies for $\nu=0$ and 1 are *lower* than those measured for the NO fragment from dissociation on the clean surface.

4. NO vibrational energy

The vibrational population distributions in Table I are obtained directly by digital integration of rotationally resolved lines. For the $\nu=2$ and 3 spectra, low intensities required digital integration over spectrally congested regions. Inspection of Table I reveals that the NO vibrational distribution from NO_2 dissociation on the O-covered surface is "colder" than that observed on the clean surface.⁵ Although the vibrational energies are colder for the O-covered surface, the enhanced yield enabled detection of the $\nu=3$ population, which fell below detection limits for the clean surface. Thus we see an overall reduction, relative to the clean surface, in the vibrational content of the NO product when the NO_2 dissociation takes place on the O-covered surface.

IV. DISCUSSION

Several effects of O coadsorption on NO_2 dissociation on Pt(111) have been observed and highlighted in the preceding section and can be summarized as follows. (1) A large (a factor of 26) enhancement in the specific dissociation yield. (2) A pronounced loss of both the low- and high-energy features of the NO E_{trans} distribution. (3) No appreciable variation in NO E_{trans} as a function of vibrational or rotational (for $J < 20.5$) quantum number. (4) A reduction in both the rotational and vibrational energy content of the NO fragment. (5) A notable propensity to populate the upper $\Omega=\frac{3}{2}$ level of the spin-orbit-split $NO^2\Pi_{\Omega}$ ground state. Most of these results can be understood in terms of a simple model based on the proposal that the excitation lifetime(s) can be enhanced by

electron-withdrawing coadsorbates which reduce substrate charge-transfer screening into antibonding molecular levels of the NO_2 adsorbate.

Whereas the above coadsorbate effects are electronic in nature, the detection of the ground-state (3P_J) atomic oxygen fragment above the surface is clearly a geometrical effect. We see that the $O(^3P_J)$ yield, aside from lifetime effects discussed below, is entirely derived from the N-bonded adsorbate which only occurs due to bridge site blocking by the preadsorbed O.

A. Primary excitation

Our assignment of the dominant excitation(s) involved in the stimulated dissociation of NO_2 on O-covered Pt(111) is based in part on the ~ 10 -eV threshold which is observed for the production of the NO and $O(^3P_J)$ fragment (see Figs. 8 and 9). In our previous analysis of NO_2 dissociation on clean Pt(111) we found that the dissociation threshold was also ~ 10 eV and suggested that $3b_2^{-1}$ and $1a_2^{-2}$ excitations are responsible.⁵ The latter assignments are based on lifetime considerations and the energy-level diagram shown in Fig. 11, which is derived from the ultraviolet photoelectron spectrum (UPS) of NO_2 on Pt(111).³⁸

It is important to note that it was previously assumed that NO_2 binds to the surface in a covalent manner such that the partially occupied $6a_1$ orbital hybridizes with the substrates.⁵ The adsorbed molecule would be approximately neutral in the ground state ($\sim 6a_1^1$), and screening charge would increase $6a_1$ occupancy in excited states with valence holes. The covalent bonding assumption on the clean surface is supported by the side-bonded geometry,²⁵ where maximal $6a_1$ -metal overlap occurs. The covalent bonding of NO_2 to the surface in the presence of preadsorbed O atoms may not be necessarily correct. It is possible that it is bonded ionically as $NO_2^-.$ There are several reasons for this counter-intuitive notion: (1) NO_2 has a large electron affinity [~ 2.3 eV (Ref.

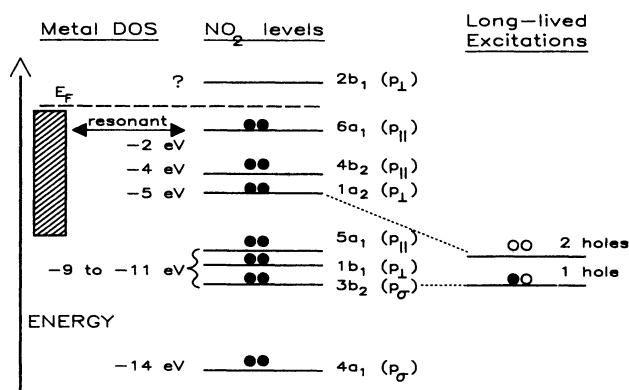


FIG. 11. Schematic energy-level diagram of NO_2 adsorbed on Pt(111). The assignments are based on the UPS spectra of Bartram and Koel (Ref. 38). The relevant atomic-orbital symmetry families (\parallel, \perp, σ , discussed in Ref. 5) from which the molecular orbitals are composed are also indicated. The molecular-orbital occupancies would be for $NO_2^-.$

39)]. (2) There is extensive site blocking by the preadsorbed oxygen atoms and a high O coverage induces a surface Madelung potential which would add to the stability of negative ions at select sites. (3) Vibrational spectra are consistent with NO_2^- frequencies.²⁴ (4) The UPS spectra of NO_2 coadsorbed with $\Theta_{\text{O}}=0.75$ ML on Pt(111) (Ref. 38) compares reasonably well with both the photoelectron spectra of solid KNO_2 (Ref. 40) and the photoemission spectra reported by Kiskinova, Pirug, and Bonzel, which appears to be NO_2^- coadsorbed with 0.15 ML of potassium on Pt(111).⁴¹ If NO_2 is adsorbed as a negative ion, then the $6a_1$ would be fully occupied ($6a_1^2$) and any screening charge must necessarily occupy the higher antibonding $2b_1$ orbital (2.5 eV above the $6a_1$ orbital in the gas-phase⁴²). However we emphasize that, except for the role of the $2b_1$ in screening the primary excitation, the remaining discussion is *independent* of the adsorbate charge state.

We see from Fig. 11, that the longest-lived excitations are those which are not degenerate with the substrate valence band, and thus must undergo intramolecular Auger decay. In order to understand the relative rates of Auger decay processes for valence excitations in NO_2 , molecular-orbital (MO) symmetries must be briefly discussed. As in Ref. 5, the MO's indicated in Fig. 11 fall into three general "families." The dominant type of atomic orbitals which make up the MO's are indicated at the right of the MO label. Here p_1 indicates $2p$ orbitals perpendicular to the molecular plane, p_σ indicate orbitals in the plane and approximately along the N-O bond axes, and p_\parallel indicates orbitals in the plane and nearly perpendicular to the bond axes. Since intramolecular Auger decay involves electrons in these orbitals, the *fastest* Auger decay occurs when a valence hole in a particular MO is filled by an electron from a higher MO of the same family, i.e., which is made up of the *same* atomic orbitals (but with different phases). Examining Fig. 11, we see that a hole in one of the levels near the ~ 10 -eV threshold, i.e., the $3b_2^{-1}$, will be much longer lived than either the $1b_1^{-1}$ or the $5a_1^{-1}$, because no higher-occupied orbital of that atomic-orbital (AO) family (p_σ) exists. This fact is not altered by partial filling of the $2b_1$ or the nature of bonding to the substrate.

Similar arguments can be applied to the $1a_2^{-2}$ excitation since it also has no higher occupancy of the same family in the covalent bonding case (no $2b_1$ occupancy). We estimate the energy of this excitation to be $2E(1a_2^{-1})+U=10-13$ eV. This estimate is based on Auger spectral analyses of other small chemisorbed molecules^{43,44} and includes a U (the screened hole-hole repulsion energy) of $\sim 2-3$ eV. This U is necessary in order to pull the second ionization potential of the $1a_2$ orbital below the valence band and hence prevent resonant decay of the two-hole excitation.⁴³

While the two-hole excitation cross section, created by shakeoff or Auger decay of deeper single holes, is about an order of magnitude lower than the one-hole cross section, it was argued⁵ that a $1a_2$ hole, being of the p_1 family, is longer lived than a $3b_2$ hole. This is because strict orthogonality exists between the AO's which make up a

$1a_2$ hole (in the p_1 family) and the AO's of the filling electron, while only approximate orthogonality exists for the case of a $3b_2$ hole. The resulting factor of $1/(2l+1)^2 = \frac{1}{25}$ in the Auger rate, due to the necessity of transferring two units of angular momentum between the p_x and p_y atomic orbitals, considerably lengthens the $1a_2$ two-hole lifetime. Thus it is reasonable that the $1a_2^{-2}$ and $3b_1^{-1}$ excitations have comparable dissociation cross sections. In fact, it will be shown in the next section that the preadsorbed oxygen can increase the lifetime of the $1a_2^{-2}$ much more than that of the $3b_2^{-1}$.

B. Charge-transfer screening and lifetimes

Clearly, electronegative O atoms will reduce substrate charge-transfer screening. However, the lifetime of the deep-valence $3b_2^{-1}$ excitation is *not* expected to be significantly altered by changes in $6a_1$ or $2b_1$ occupancy since it is energetically allowed to Auger decay using electrons from other levels (e.g., $4b_2$ or $1a_2$). In contrast, shallower excitations such as the $1a_2^{-2}$ must decay using the screening electrons, and thus are strongly affected by the degree of charge-transfer screening. With regard to other two-hole excitations, the argument for $1a_2^{-2}$ dominance is weakened if the $2b_1$ level is occupied, since it has the same symmetry. In this case, excitations such as $4b_2^{-2}$ and $4b_2^{-1}1a_2^{-1}$ would contribute. Even in the case of significant $2b_1$ occupancy, however, oxygen would still strongly affect the two-hole excited-state lifetime(s) by reducing substrate screening. Since both the $3b_2^{-1}$ and two-hole excitations apparently have comparable yields in the absence of preadsorbed oxygen, we suggest that the O-induced reduction of screening charge causes a strong increase of the two-hole-excitation lifetimes relative to the $3b_2^{-1}$.

C. Dynamical effects

In stimulated desorption and dissociation, final-state distributions are determined by *both* the initial ground-state wave function and by the time evolution of the molecular wave function under the influence of the repulsive excited-state potential-energy surface. The extent of the influence of the excited-state potential is dependent upon both its topography and the excited-state lifetime. The two-hole excitations ($1a_2^{-2}$, etc.) involve nonbonding molecular orbitals. Thus, apart from hole-hole repulsion, most of the bond-breaking force must arise from the presence of the antibonding ($6a_1$ or $2b_1$) screening charge which is transferred to the molecule from the substrate. The dissociation is somewhat analogous to gas-phase photodissociation, which results from nonbonding-to-antibonding electronic excitations.

Changes in dissociative excited-state forces resulting from variations in screening-charge density are distinctly reflected in the fragment E_{trans} distributions. The reduction of screening charge by the presence of the O atoms and, possibly, the change to a N-bonded coordination can "flatten" the excited-state potential-energy surface. The striking collapse of the *high-energy* features in the E_{trans}

distributions of the NO (both $\Omega = \frac{1}{2}$ and $\frac{3}{2}$) fragment supports the idea that a reduction of excited-state force(s) is brought about by diminished screening. The disappearance of the *low-energy* tail can also be due to a reduced force, as well as an increased lifetime of the excitation(s).^{6,23} Our present results clearly show that in the case of NO₂ dissociation on O-covered Pt(111) *both* the dissociation forces and excitation lifetimes change. Thus we have an interesting counterbalance between the increased lifetime vs reduced dissociative forces when the screening population is reduced. We see that small changes in lifetimes have larger consequences on the yield than the reduction of excited-state force(s). This is expected since $\ln Y \sim \Gamma f$, where the dissociation yield is Y , the lifetime $\Gamma \propto 1/q^2$, the force $f \propto q$, and the screening charge is q .^{45,46}

D. Internal energy distributions

Vibrational and rotational excitation of the NO fragment are expected since the screening charge occupies an antibonding molecular level, increasing NO bond lengths and decreasing ONO bond angles.⁵ The results in Table I show that both vibrational and rotational excitation occur, but that for NO₂ dissociation on the O-covered surface, the NO internal energies are *lower* than those for dissociation on the clean surface. The lower internal energies are certainly consistent with the reduced excited-state forces due to diminished screening.

It is not clear, however, how much the NO rotational energy is affected by the dominant two-hole excitation(s) on the O-covered surface and by anisotropic surface scattering as discussed by Hasselbrink.⁴⁷ The latter is perhaps manifested by the increase in the NO E_{trans} distributions with $J > 20.5$ (Fig. 6). Although inelastic scattering on both the excited and ground-state potentials is expected, the translational-rotational coupling is only observable at high J . A similar shift in translational energy with high angular momentum has been observed in the ESD of NO coadsorbed with $\Theta_{\text{O}} = 0.75$ ML on Pt(111).²³ The shift is much more pronounced, even at low J , in laser desorption.^{3,48}

E. NO spin-orbit propensity

The observed spin-orbit propensity of $\sim 4:1$ at $J < 10.5$ for populating the upper ($\Omega = \frac{3}{2}$) rather than the lower ($\Omega = \frac{1}{2}$) level of the NO ${}^2\Pi_{\Omega}$ ground state is very similar to that observed for the ESD of NO from O-covered Pt(111) (Ref. 23) and for laser desorption of NO from clean Pt(111).³ A qualitative theory for the resonant neutralization, following Auger decay of the excitation(s), of an open-shell hindered rotor near a metal surface can explain the spin-orbit propensity observed in ESD of NO from O-covered Pt(111).²³ Critical factors relevant to that theory are as follows: (1) The presence of a strongly

spin-orbit-split substrate such as Pt, (2) an open-shell diatomic which has been temporarily ionized above the surface, and (3) a desorbate with a quantization axis which is oriented *along the surface normal* above a site with C_{3v} point-group symmetry (both atop and threefold hollow sites are C_{3v}). The strongly spin-orbit-split metal surface has a greater density of states (number of electrons) for $d\pi$ -aligned ($m_j = \frac{3}{2}$) than for $d\pi$ -antialigned ($m_j = \frac{1}{2}$).²³ Consequently, if the NO⁺ fragment is aligned along the surface normal and above a site with C_{3v} symmetry at the time of reneutralization, then the propensity would reflect the substrate density of states. It is relevant that in the laser desorption of NO from clean Pt(111), the desorbates are peaked at the surface normal.³

While not immediately obvious given the tilted NO bonds in the C_{2v} N-bonded NO₂ coordination to the surface, our results suggest a normal orientation for the departing NO fragment in the presence of the coadsorbed oxygen. This may occur if lighter O fragments leave the surface before NO; this is consistent with the crude O(³P_J) translational energies shown in Fig. 7. In this case the NO fragment may end up on a potential energy surface which is very similar to that seen in NO ESD from an O-covered surface. Indeed, the NO E_{trans} distributions from stimulated dissociation of NO₂ and ESD of NO from O-precovered ($\Theta_{\text{O}} = 0.75$ ML) Pt(111) are very similar.^{6,23} Angular-distribution studies of the dissociation fragments are currently under way; initial results indicate NO trajectories near normal to the surface.⁴⁹

V. CONCLUSIONS

We have seen a large enhancement in the NO₂ dissociation yield in the presence of coadsorbed O, along with a reduction in fragment internal energies, an inversion in the NO spin-orbit population, and a distinct narrowing of the NO translational energy distribution. The ~ 10 -eV dissociation threshold indicates that a valence excitation is created in the adsorbate which must Auger decay via the shallow, metal-adsorbate rehybridized levels. These excited states are primarily two-hole excitations (from the $1a_2$ and, possibly, the $4b_2$ levels) which Auger decay leaving temporary positive ions (NO⁺) which must be reneutralized. We believe that the strong propensity for the formation of the $\Omega = \frac{3}{2}$ level is due to the reneutralization by the spin-orbit-split substrate and that the NO⁺ is oriented normal to the surface.

These observations are similar to O-induced effects on the ESD of NO from Pt(111) (Refs. 6 and 23) and further support our general conclusion that yields and products of stimulated surface processes are very sensitive probes of coadsorbate-induced changes in excited-state lifetimes and forces. In the case of stimulated dissociation, changes in *both* the excited-state lifetime(s) and forces are evident. The enhanced yield is mainly a lifetime effect, brought about by the reduction of the screening charge used in the Auger decay of the primary excitation. How-

ever, the disappearance of the NO E_{trans} at high energy and the reduced internal energies reflect changes in the excited-state forces which are consistent with the reduction of screening. In conclusion, we have seen that stimulated dissociation, in addition to desorption, is dependent on coadsorbate-induced changes in substrate screening and rehybridization.

ACKNOWLEDGMENTS

The authors are indebted to M. E. Bartram, for allowing us to study his UPS experimental data prior to publication, and to N. D. Shinn for critical comments. This work was supported by the U.S. Department of Energy under Contract No. DE-AC04-76DP00789.

*Present address: Molecular Science Research Center K2-14, Battelle Pacific Northwest Laboratories, Richland, WA 99352.

¹A. R. Burns, E. B. Stechel, and D. R. Jennison, *Phys. Rev. Lett.* **58**, 250 (1987).

²A. R. Burns, D. R. Jennison, and E. B. Stechel, *J. Vac. Sci. Technol. A* **5**, 671 (1987).

³S. A. Buntin, L. J. Richter, D. S. King, and R. R. Cavanagh, *J. Chem. Phys.* **91**, 6429 (1989).

⁴P. D. Johnson, A. J. Viescas, P. Norlander, and J. C. Tully, *Phys. Rev. Lett.* **64**, 942 (1990).

⁵A. R. Burns, D. R. Jennison, and E. B. Stechel, *Phys. Rev. B* **40**, 9485 (1989).

⁶A. R. Burns, D. R. Jennison, and E. B. Stechel, *J. Vac. Sci. Technol. A* **8**, 2705 (1990).

⁷E. P. Marsh, M. R. Schneider, T. L. Gilton, F. L. Tabares, W. Meier, and J. P. Cowin, *Phys. Rev. Lett.* **60**, 2551 (1988); *J. Chem. Phys.* **92**, 2004 (1990).

⁸E. Hasselbrink, S. Jakubith, S. Nettesheim, M. Wolf, A. Casuto, and G. Ertl, *J. Chem. Phys.* **92**, 3154 (1990).

⁹L. Hanley, X. Guo, and J. T. Yates, Jr., *J. Chem. Phys.* **91**, 7220 (1989).

¹⁰W. Ho, *Comments Condens. Mater. Phys.* **13**, 293 (1988); W. Ho, in *Desorption Induced by Electronic Transitions, DIET IV*, edited by G. Betz and P. Varga (Springer-Verlag, New York, 1990), pp. 48-64.

¹¹X.-Y. Zhu, S. R. Hatch, A. Campion, and J. M. White, *J. Chem. Phys.* **91**, 5011 (1989).

¹²M. Wolf, E. Hasselbrink, J. M. White, and G. Ertl, *J. Chem. Phys.* **93**, 5327 (1990).

¹³P. S. Shaw, E. Sanchez, J. O'Neill, Z. Wu, and R. M. Osgood, *J. Chem. Phys.* **94**, 1643 (1991).

¹⁴Z. C. Ying and W. Ho, *Phys. Rev. Lett.* **65**, 741 (1990).

¹⁵T. M. Orlando, A. R. Burns, E. B. Stechel, and D. R. Jennison, *J. Chem. Phys.* **93**, 9197 (1990).

¹⁶M. D. Miehler and W. Ho, *J. Chem. Phys.* **91**, 2755 (1989).

¹⁷T. A. Germer and W. Ho, *J. Chem. Phys.* **93**, 1474 (1990).

¹⁸D. V. Chakarov and W. Ho, *J. Chem. Phys.* **94**, 4075 (1991).

¹⁹X.-Y. Zhu and J. M. White, *J. Chem. Phys.* **94**, 1555 (1991).

²⁰D. R. Jennison, E. B. Stechel, and A. R. Burns, in *Desorption Induced by Electronic Transitions, DIET III*, edited by R. H. Stulen and M. L. Knotek (Springer-Verlag, Berlin 1988), p. 167.

²¹Z. Gortel and M. Tsukada, *Phys. Rev. B* **39**, 11 259 (1989).

²²H. P. Bonzel, *Surf. Sci. Rep.* **8**, 43 (1987).

²³A. R. Burns, E. B. Stechel, D. R. Jennison, and T. M. Orlando, *Phys. Rev. B* **45**, 1373 (1992).

²⁴M. E. Bartram, R. G. Windham, and B. E. Koel, *Langmuir* **4**, 240 (1988).

²⁵M. E. Bartram, R. G. Windham, and B. E. Koel, *Surf. Sci.* **184**, 57 (1987).

²⁶J. Segner, W. Vielhaber, and G. Ertl, *Isr. J. Chem.* **22**, 375 (1982).

²⁷D. H. Parker, M. E. Bartram, and B. E. Koel, *Surf. Sci.* **217**, 489 (1989).

²⁸Gerhard Herzberg, *Spectra of Diatomic Molecules*, 2nd ed. (Van Nostrand Reinhold, New York, 1950), pp. 264 and 558.

²⁹D. C. Jacobs, R. J. Madix, and R. N. Zare, *J. Chem. Phys.* **85**, 5469 (1986).

³⁰L. T. Earls, *Phys. Rev.* **48**, 423 (1935).

³¹J. E. M. Goldsmith, *J. Chem. Phys.* **78**, 1610 (1983).

³²T. M. Orlando, A. R. Burns, E. B. Stechel, and D. R. Jennison, *J. Vac. Sci. Technol. A* **9**, 1769 (1991).

³³M.-R. Taherian, P. C. Crosby, and T. G. Slinger, *J. Phys. Chem.* **91**, 2304 (1987).

³⁴S. T. Pratt, P. M. Dehmer, and J. L. Dehmer, *Phys. Rev. A* **43**, 282 (1991).

³⁵T. G. Slinger, W. K. Bischel, and M. J. Dyer, *J. Chem. Phys.* **79**, 2231 (1983).

³⁶W. J. van der Zande, R. Zhang, H.-G. Rubahn, M. J. Bronikowski, and R. N. Zare (unpublished).

³⁷Y.-L. Huang and R. J. Gordon (unpublished).

³⁸M. E. Bartram and B. E. Koel (unpublished).

³⁹K. M. Ervin, J. Ho, and W. C. Lineberger, *J. Phys. Chem.* **92**, 5405 (1988).

⁴⁰M. Considine, J. A. Conner, and I. H. Hillier, *Inorg. Chem.* **16**, 1392 (1977).

⁴¹M. Kiskinova, G. Pirug, and H. P. Bonzel, *Surf. Sci.* **140**, 1 (1984).

⁴²W. Zhang, K. H. Sze, C. E. Brion, X. M. Tong, and J. M. Li, *Chem. Phys.* **140**, 265 (1990).

⁴³E. Umbach and Z. Hussain, *Phys. Rev. Lett.* **52**, 257 (1984).

⁴⁴B. E. Koel, J. M. White, and G. M. Loubriel, *J. Chem. Phys.* **77**, 2665 (1982).

⁴⁵E. B. Stechel and M. L. Knotek, *Surf. Sci.* **167**, 297 (1986).

⁴⁶D. Menzel and R. Gomer, *J. Chem. Phys.* **41**, 3311 (1964).

⁴⁷E. Hasselbrink, *Chem. Phys. Lett.* **170**, 329 (1990).

⁴⁸P. M. Ferm, F. Budde, A. V. Hamza, S. Jakubith, D. Wiede, P. Andresen, and H. J. Freund, *Surf. Sci.* **218**, 467 (1989).

⁴⁹A. R. Burns, E. B. Stechel, and D. R. Jennison (unpublished).